Versatile X-ray operando electrolysis cell

Asger B. Moss[a], Joel Hätinen[b, c, d], Peter Kůš[e], Sahil Garg[a], Marta Mirolo[b], Ib Chorkendorff[a], Brian Seger[a], Jakub Drnec[b, *]

[a]*Surface Physics and Catalysis (Surf Cat) Section, Department of Physics, Technical University of Denmark, 2800 Kgs. Lyngby, Denmark*

[b]*Experimental Division, European Synchrotron Radiation Facility, Grenoble, France*

[c]*Department of Mathematics and Systems Analysis, P.O. Box 11100, FI-00076, Aalto University, Finland*

[d]*Helsinki Institute of Physics, P.O. Box 64, FI-00014 University of Helsinki, Finland*

[e]*MFF, UK, Prague, Czech Republic*

**Corresponding author: Jakub Drnec, Email: drnec@esrf.fr*

Abstract

We here present a design for a versatile electrochemical cell designed for X-ray operando studies of Membrane Electrode Assembly (MEA) based electrolysis. The cell has been tested for CO_2 electrolysis performance and for various X-ray techniques.

Introduction

In the quest for a fossil-free world electrification has become a cornerstone in the strategy, and electrolysis appears to be a promising route for energy storage and renewable feedstock of chemicals[1]. So far, most research has been in the field of water electrolysis[2], but lately, the electrolysis of more complex reactions, such as CO_2 reduction reaction (CO_2RR[1,3]), has gained interest. In both water electrolysis and especially in CO_2 (and CO) electrolysis one of the most promising cell designs is the zero-gap membrane electrode assembly (MEA) due to a low operating potential and a simple configuration[4–6]. From a research perspective, the MEA does though come with challenges. MEAs are inherently difficult to study in situ and in operando conditions, and even postmortem analysis is relatively difficult as the assembly often suffers from mechanical instability when disassembled. With

the development of 4th Generation synchrotrons, such as the European Synchrotron Radiation Facility Extremely Brilliant Source (ESRF-EBS), it is possible to obtain a micro-sized beam at high energy and flux, which can be used to investigate the MEA at grazing incidence geometry (beam is parallel to the catalyst surface) during operation. This not only gives a much larger interaction volume compared to the situation where the beam is perpendicular to the catalyst layer, but it also provides the possibility to investigate different MEA depths, ie. enode and cathode GDEs, membrane, thin catalystlayer etc. by moving the cell in the beam through a scanning method as illustrated in Figure 1. However, the typical MEA cell cannot be used for X-ray operando experiments in this geometry, as this sets certain requirements regarding the cell shape and materials. Even though there exist many cells for X-ray experiments[7], most of them are either not suitable for investigating MEAs for water splitting and CO_2 reduction experiments. Typically they are either significantly smaller than the typical cell, very challenging to assemble or designed for use with the beam perpendicular to the GDE. Therefore, this work aimed at designing a cell that is both easy to work with, suitable for multiple applications and can be used for a large variety of X-ray techniques, including Wide/Small Angle X-ray Scattering (W/SAXS), diffraction and absorption tomography, X-ray dark-field microscopy and possibly even coherent scattering experiments using high energy X-ray probe. While the cell can be used in many applications, in the following we will focus on the performance towards CO_2RR to discuss the cell capabilities.

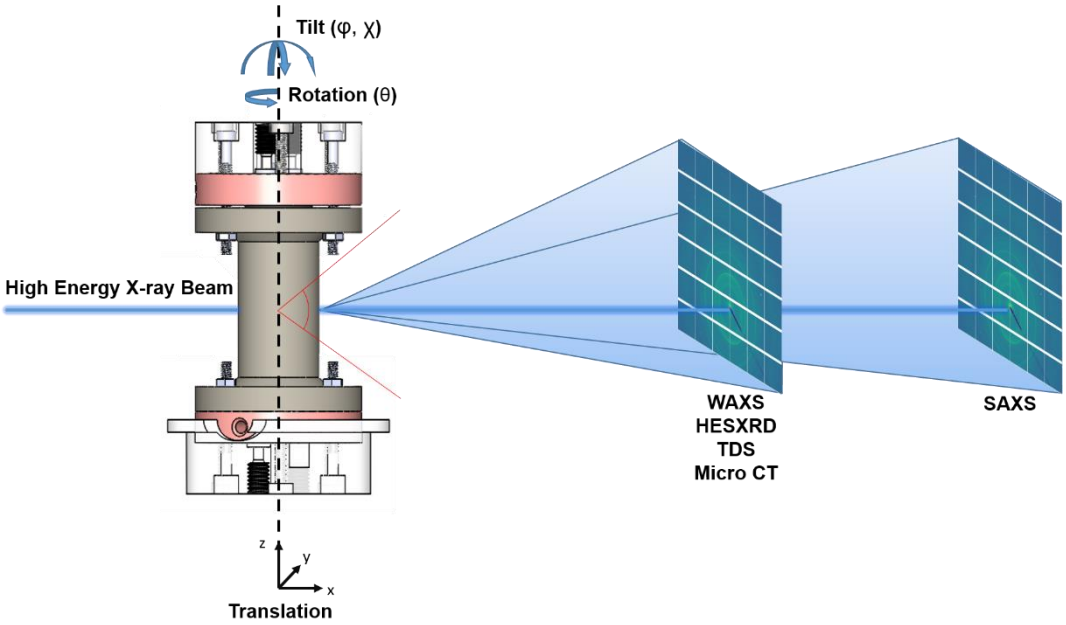

Figure 1 Illustration of the cell in the beam path. The cell can be moved in the beam (through translation and tilting) allowing for the different parts of the MEA to be investigated. The cell design

allows X-rays scattered in very wide angles to exit unhindered as illustrated by the red lines. The circular design and the possibility to rotate it freely also enables the cell to be used for tomography experiments.

Result and Discussion

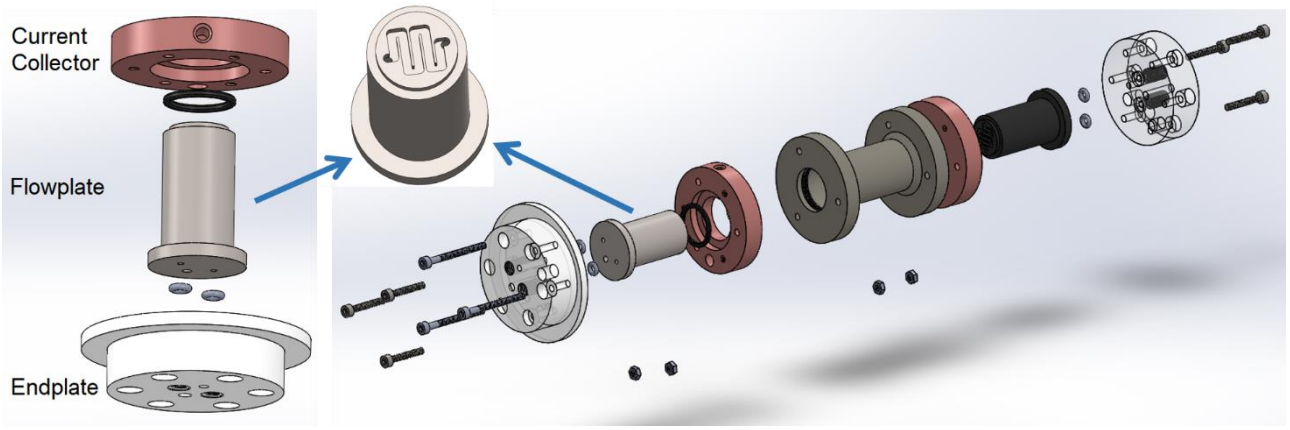

Figure 2 Left: Exploded view of the anode flowfield. Right: Exploded view of the whole cell. The insert shows the flowplate with the single-channel serpentine.

Cell design

The cell consists of three main parts; an anode and cathode flowfields and a polyether-ether ketone (PEEK) casing in which the two flowfields are inserted from each end (Figure 1). Each flowfield consists of a 3D printed endplate in which the gas/liquid tubes are connected, a flowplate[1] of suitable material, eg. graphite, Ti, or stainless steel, and anodic and cathodic current collectors, which also serve the purpose of fastening the flowplate to the endplate.

Unlike the typical MEA electrolyzer, the cell has a dog bone shape, with the MEA being placed in the middle. The design is chosen in order to have a wide opening without any blockage of the scattered X-rays making it possible to measure very wide angles and thereby a large portion of the reciprocal space. This is indicated by the red line in Figure 1. The circular design was chosen to enhance tomography capabilities by minimizing potential reconstruction defects. Sealing between the

[1] To avoid confusion the term flowplate is used for the raw piece, whereas the assembly of the endplate, flowplate and current collector is called flowfield.

flowfield and the membrane is ensured by a Viton O-ring which is slightly lowered into the flowfield. As the O-rings in the two flowfields are not fully submerged, a gap is created when the two flowfields are pushed together. This gap ensures that the GDEs are not compressed too much.

The inner diameter of the O-ring is 9 mm leaving room for a disk-shaped GDE with a 63.6 mm^2 area. The diameter of the cell is small enough to allow for high-energy X-ray imaging, scattering, and tomography experiments with sufficient contrast and resolution and with no noticeable issues related to significant peak broadening, secondary scattering, parallax effect, and absorption. At the same time, the electrode area is still of a size comparable to most experimental work in the CO_2E and water electrolysis fields thus allowing investigations that are relevant to commercial devices.

In order to obtain the dog bone shape, the flowplates are shaped as rods with a collar for fixation and a pin for alignment in one end and channels going through to the other end where a serpentine flow channel ensures gas or liquid transfer to the GDE. The flow channel geometry was chosen in this case to be a single channel serpentine with fairly wide channel dimensions. Though the geometry of the flow path is known to be important in electrolysis devices[8], a simple design was chosen both to minimize blockage from any salt deposition that may occur on the gas fed side of the device and to enhance bubble removal. This design also allows for unhindered x-ray analysis of the part of the GDE that might bulge into the serpentine. The channels are 1 mm deep, 1.25 mm wide, and 5.6 mm long and the lands are 0.25 mm. The exact geometry can be seen in the insert of Fig. 1. The flowfield assembly is designed in a way that it allows easy flowplate exchange, so the flowplate can be manufactured from different materials and with different channel geometry.

The current collector is a Cu ring with a chamfer fitting the collar of the flowplate such that when assembled they form a flush surface towards the endplate. A hole in the side of the current collector can be used to connect to a potentiostat.The flowplate and current collector are firmly attached to the endplate by three screws that go through the endplate into the threads in the current collector. Two alignment pins ensure that the three parts are fixed and that the gas/liquid channels are placed correctly. Two small O-rings slightly submerged into the endplate creates a sealed connection and presses the collar of the flowplate towards the current collector to ensure good electrical connection.

Our initial design used metal quick connectors for the connection of gas and electrolyte tubes into the flowfields, but initial tests of CO_2E with a silver catalyst indicated a rapidly increasing H_2 selectivity with time. While the CO_2RR selectivity could be regained temporarily by a nitric acid wash of the cell, the following experiments always resulted in a similar performance loss. It is believed this H_2

selectivity increase was related to contamination from the metal quick connectors (most likely from Ni coming off the steel). The metal inlets were exchanged with 1/16" PTFE tubes inserted through the endplate. Further tests did not show the rapid increase in H_2 selectivity, thus resolving this issue. A pressure-tight sealing was made using IDEX SuperFlangeless flat bottom ferrules (M-644-03, M-650). The inlet tube is extended beyond the ferrule and partially into the o-rings, thus sealing the side towards the flowplate. This sealing avoids the gas/liquid contacting the endplate or any metal part except the flowplate itself.

We expect the overall cell design to be capable of working under both highly acidic as well as alkaline conditions, since all gaskets can be exchanged depending on the specific use, and similarly the flowplates can be manufactured in a large variety of materials, with good electrical conductivity being the only general requirement. It should be noted that only neutral and moderately alkaline conditions were tested.

Assembly

Due to the long casing, assembling the cell has substantial complexities. When assembliyng the cell, the membrane is first inserted slightly into the casing ant and then pushed all the way in using the flowplate with the GDE placed on top. In order to stabilize the membrane upon insertion, we used a 200 µm thick gasket (3-D printed from Stratasys VeroClear RGD810) that is placed on the anode side as the membrane otherwise tends to stick to the side when inserted. The gasket eases the assembly significantly and allows relatively consistent results. In case the 3D print material should not be compliant with the experiment performed, a gasket of different material can be choosen. We have sucsessfully tested both PTFE, PFA and FEP gaskets of similar dimension. When fully inserted, the flowplate is tightened flush to the casing. This ensures that the height of the MEA is always the same making further alignment easier. The cell is then rotated 180 degrees so the cathode flowfield can be inserted with the cathode GDE lying on the top. The compression of the MEA is controlled by the tightening of the cathode flowfield to the casing.

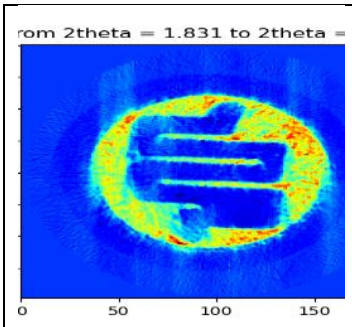	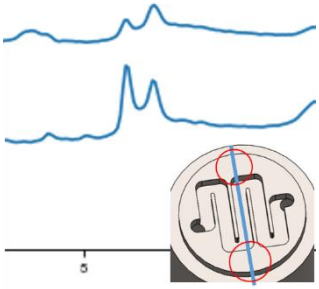	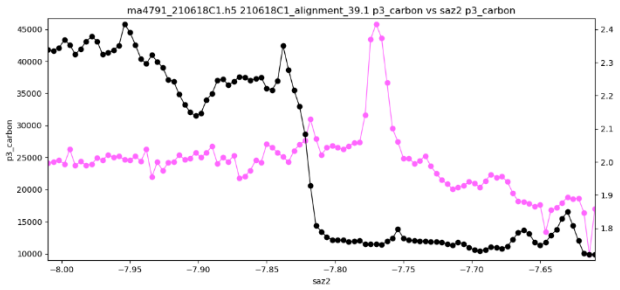
Figure 3 a) An example of an x-ray tomography taken at the height of the graphite flow channel.	b) example of a peak split from the graphite flowplate. The split comes when the beam diffracts on the two outer edges of the serpentine (reds circles), as these are distanced differently from the detector.	c) An example of how the surface of the land in the flow channel can be used to align the cell. The more stepped the black line is, the more in plane the cell is with the beam. The pink line shows the Cu content indicating the height of the catalyst layer.

Alignment

The alignment of the cell is important in order to be able to investigate the different layers of the MEA correctly. The cell is mounted in a 6-axis alignment stage so it can be moved tilted and turned freely in all directions (x, y, z, θ, φ, χ), and thereby be aligned so the MEA is parallel to the beam. By using the polished land surface of the flowplate channels, it is possible to slowly tilt the cell, while scanning the height of the cell, until the signal from the surface of the land shows the steepest step function as shown by the example in Figure 3d. In order to minimize this iterative procedure, we have equipped the anode endplate with an edge fitting down in the holder. This gives a rough initial alignment of the cell.

Peak splitting and broadening

When scanning along the flow channels, we observed a set of split peaks from the graphite flowfield. The split occurs because the two ends are distanced differently from the detector, so-called parallax effect. (Fig. 2 b). The same effect is expected to occur with other elements of the cell, e.g. the catalyst layer, but here it will be seen as a peak broadening. This is one of the limitations of the cell that one

should be aware of, but this can be accounted for during the post-processing of the data[9] and including this effect during the calibration of instrumental parameters.

Diffraction Tomography

We tested the cell to be used in a diffraction tomography experiment, and found it highly suitable for the purpose. An example can be seen in fig. 2 a). In such characterization, the pencil beam is scanned along the cell at different azimuthal angles, allowing reconstruction of the full diffraction pattern for each real-space voxel [10–12] The circular geometry and relatively small width speeds the measurement process and it possible to obtain an acceptable resolution (down to the size of the X-ray beam) with a reasonable acquisition time. However, we do in some cases observe damage to the center of the membrane after the tomography scans. While this can limit the tomography possibilities to an extent, carefully selected experimental conditions with respect to the total X-ray dose can mitigate this issue.

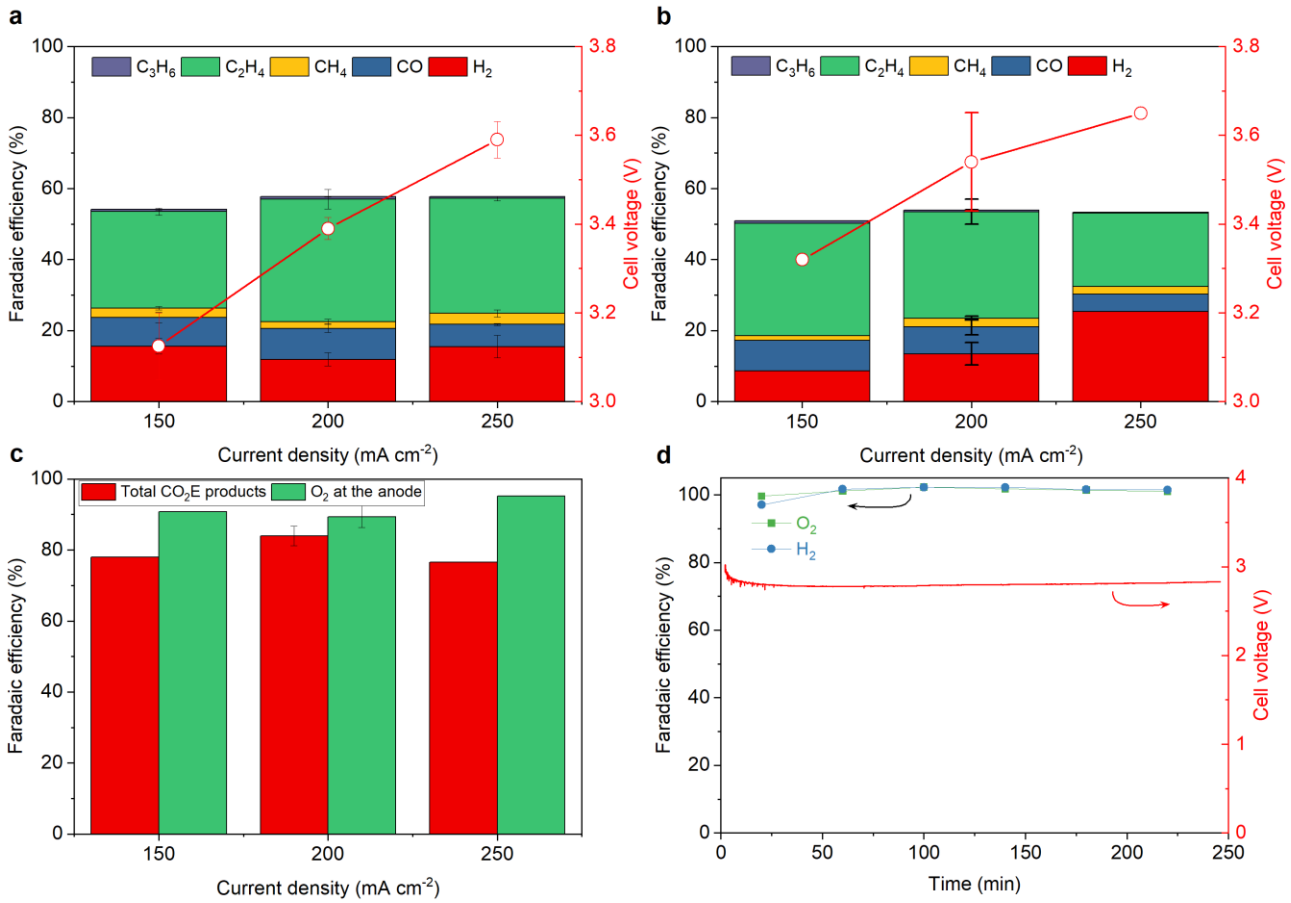

Figure 4 Comparison of electrocatalytic performance in terms of FE of gaseous cathodic products and cell potential over sputtered Cu GDEs (150 nm) in a MEA electrolyzer tested separately at two different locations: (a) without X-rays at DTU and (b) with X-rays at ESRF; (c) Comparison of total FE of CO_2RR products versus FE of O_2 at the anode in experiments performed during X-ray irradiation at ESRF; (d) shows an experiment where Ar was used instead of CO_2 showing a non-corroding anode as the H_2 and O_2 FEs are both 100%; The error bars in (a) show the standard deviation of three separate experiments where the 2nd GC injection was used to calculate the FE, while, the error bars in (b and c) for 200 mA·cm^{-2} show the standard deviation of four separate experiments. 150 and 250 mA·cm^{-2} experiments shown in (b) (at ESRF) were only performed once due to time limitations.

Electrochemical Testing

In order to test if the electrolyzer can achieve commercially relevant current densities (≥ 200 mA·cm^{-2}) for CO_2 reduction, we investigated the electrocatalytic performance of sputtered Cu GDEs at different current densities. **Figure 4**a shows that our MEA electrolyzer can produce a reasonable level of gaseous CO_2RR products including CO, CH_4, C_2H_4, C_3H_6, and H_2 during the initial stages of testing

(Data taken after 30 min of operation). We also see no indication that high energy (69 keV) X-ray illumination alters the electrocatalytic performance significantly. Figure 4a and 4b show the cell performance in terms of faradaic efficiencies of gaseous products and cell potentials, with (4a) and without (4b) X-rays, at different current densitieswith all operating conditions such as catalysts (both cathode and anode GDE), AEM, and electrolyte kept identical. Furthermore, the experiments tested without X-rays were done at the Technical University of Denmark (DTU) whereas the x-ray irradiated experiments were done at the ID31 beamline of the European Synchrotron Radiation Facility (ESRF), demonstrating the reactor system is robust towards practical laboratory variations as well. In both cases in Figure 4a and 4b, the total FE of products does not reach 100%. The explanation is mainly that the data does not include liquid product analysis. Figure 4c shows the total FE of CO_2RR products (red bars) at different current densities, including liquid products collected at the end of the experiment. With liquid product analysis being the total production of a 3 hr experiment, and the gas products being the average of the continuous GC injections, the total faradaic efficiency is an estimated average of the entire experiment and we do therefore not expect the data to match 100% perfectly. The fact that the total FE gets to around 80% and not higher shows that there is still a significant fraction of the current not accounted for. To account for the missing charge, we calculated the FE of oxygen (O_2) at the anode because if part of the CO_2RR products crosses the membrane and gets oxidized at the anode then the O_2 faradaic efficiency should also decrease. If we assume full anodic oxidation to CO_2, then there would be a one-to-one relationship between unaccounted faradaic efficiency at the cathode and non-O_2 evolution faradaic efficiency at the anode. This principle also assumes a non-corroding anode, which we show to be the case in **Figure 4**d where Ar was used instead of CO_2 so the only cathode reaction was HER. Here the faradic efficiencies of both H_2 and O_2 are 100%. Since the experiments with x-rays appeared to show the most substantial unaccounted for products, we analyzed the anodic O_2 evolution faradaic efficiency of these experiments. Despite **Figure *4***c confirming our hypothesis that O_2 faradaic efficiency at the anode does not reach 100% (and thus CO_2RR products are being oxidized) when comparing this to the total faradaic efficiency of CO_2E products as in **Figure *4***c, there is still a missing 5 to 15% FE. Evaporated liquid products (e.g. ethanol) were not analyzed at either the cathode or anode, which are potential sources for the missing faradaic efficiency.

Typically, water electrolyzers operate at current densities[13] one order of magnitude higher, but we have not attempted to benchmark the cell for water electrolysis at these currents.

Methods

MEA setup and electrochemical measurements

For CO2 electrolysis, a dry CO2 gas (5N) was fed to the cathode flow-field at 30 sccm using a mass flow controller (Vöegtlin red-y smart series), and 60 ml of 0.1 M KHCO3 anolyte was circulated at the anode using a digitally controlled diaphragm pump (KNF NF1.5TTDCB-4) set at 25% of its maximum speed (which roughly corresponds to 7.5 ml/min). For the cathode, a 150 nm layer of 6N sputtered Cu was deposited onto Sigracet 39 BB (Fuelcell Store), while, for the anode, a commercial IrO2-based GDE (from Dioxide Materials, USA) was utilized. In all the experiments, an anion exchange membrane (Sustainion X37-50, Dioxide Materials, USA) activated in 1 M KOH solution and later kept in deionized water was used.All electrochemical experiments were performed in a two-electrode setup at a constant current. Current density of 150, 200, and 250 mA/cm2 were applied during galvanostatic measurements using a potentiostat (Biologic SP-300 and SP-240). For selectivity/faradaic efficiency calculations, the gaseous products formed at the cathode (and pre-washed into a deionized water chamber) were injected into an online GC (Agillent 6890A) equipped with a flamed ionization detector with a methanizer and a thermal conductivity detector for the detection of CO, CH4, C2H4, C3H6, and H2, respectively. High-purity argon (5N, Linde Denmark) was used as the carrier gas. The liquid products both collected at the cathode and the anode were detected using a liquid chromatograph (Agilent 1260 Infinity II) with 0.1 M KHCO3 as a reference solution and 0.05 M H2SO4 as the internal solvent.

Conclusion

We have presented a design for an electrolysis cell suitable for both water and CO2 electrolysis with a geometric area large enough to be comparable to other cells, and with a design that allows for various X-ray diffraction and scattering techniques including tomography. The cell design has shown high repeatability in the electrochemical measurements, manageable X-ray background at high energies, and sufficiently easy assembly, in order to study electrochemical processes in MEAs at high current densities.

References

1. Nitopi, S. *et al.* Progress and Perspectives of Electrochemical CO 2 Reduction on Copper in Aqueous Electrolyte. *Chem. Rev.* **119**, 7610–7672 (2019).

2. Carmo, M., Fritz, D. L., Mergel, J. & Stolten, D. A comprehensive review on PEM water electrolysis. *Int. J. Hydrogen Energy* **38**, 4901–4934 (2013).

3. Lu, Q. & Jiao, F. Electrochemical CO2 reduction: Electrocatalyst, reaction mechanism, and process engineering. *Nano Energy* **29**, 439–456 (2016).

4. Weng, L. C., Bell, A. T. & Weber, A. Z. Towards membrane-electrode assembly systems for CO2 reduction: A modeling study. *Energy Environ. Sci.* **12**, 1950–1968 (2019).

5. Ge, L. *et al.* Electrochemical CO2 reduction in membrane-electrode assemblies. *Chem* vol. 8 663–692 (2022).

6. Lees, E. W., Mowbray, B. A. W. W., Parlane, F. G. L. L. & Berlinguette, C. P. Gas diffusion electrodes and membranes for CO2 reduction electrolysers. *Nat. Rev. Mater.* **7**, 55–64 (2022).

7. Farmand, M. *et al.* Electrochemical flow cell enabling operando probing of electrocatalyst surfaces by X-ray spectroscopy and diffraction. *Phys. Chem. Chem. Phys.* **21**, 5402–5408 (2019).

8. Olesen, A. C., Rømer, C. & Kær, S. K. A numerical study of the gas-liquid, two-phase flow maldistribution in the anode of a high pressure PEM water electrolysis cell. *Int. J. Hydrogen Energy* **41**, 52–68 (2016).

9. Vamvakeros, A. *et al.* DLSR: A solution to the parallax artefact in X-ray diffraction computed tomography data. *J. Appl. Crystallogr.* **53**, 1531–1541 (2020).

10. Harding, G., Kosanetzky, J. & Neitzel, U. X-ray diffraction computed tomography. *Med. Phys.* **14**, 515–525 (1987).

11. Kleuker, U., Suortti, P., Weyrich, W. & Spanne, P. Feasibility study of x-ray diffraction computed tomography for medical imaging. *Phys. Med. Biol.* **43**, 2911 (1998).

12. Bleuet, P. *et al.* Probing the structure of heterogeneous diluted materials by diffraction tomography. *Nat. Mater. 2008 76* **7**, 468–472 (2008).

13. Grigoriev, S. A., Fateev, V. N., Bessarabov, D. G. & Millet, P. Current status, research

trends, and challenges in water electrolysis science and technology. *Int. J. Hydrogen Energy* **45**, 26036–26058 (2020).